

# Studying 21cm power spectrum with one-point statistics

Hayato Shimabukuro<sup>1,2</sup>, Shintaro Yoshiura<sup>2</sup>, Keitaro Takahashi<sup>2</sup>, Shuichiro Yokoyama<sup>3</sup> and Kiyotomo Ichiki<sup>1</sup>

<sup>1</sup>*Department of Physics, Graduate School of Science, Nagoya University, Aichi, 464-8602, Japan*

<sup>2</sup>*Department of Physics, Kumamoto University, Kumamoto, Japan*

<sup>3</sup>*Department of Physics, Rikkyo University, Tokyo, Japan*

1 June 2015

## ABSTRACT

The redshifted 21cm line signal from neutral hydrogens is a promising tool to probe the cosmic dawn and the epoch of reionization (EoR). Ongoing and future low-frequency radio experiments are expected to detect its fluctuations, especially through the power spectrum. In this paper, we give a physical interpretation of the time evolution of the power spectrum of the 21cm brightness temperature fluctuations, which can be decomposed into dark matter density, spin temperature and neutral fraction of hydrogen fluctuations. From the one-point statistics of the fluctuations, such as variance and skewness, we find that the peaks and dips in the time evolution are deeply related to X-ray heating of the intergalactic gas, which controls the spin temperature. We suggest the skewness of the brightness temperature distribution is a key observable to identify the onset of X-ray heating.

**Key words:** cosmology: theory — intergalactic medium — Epoch of Reionization — 21cm line

RUP-14-18

## 1 INTRODUCTION

At the early epoch of the universe ( $z \sim 1100$ ), proton couples with free electron, which is called “recombination” and neutral hydrogen is formed. After recombination, the universe keeps neutral state until first object is formed. We call this epoch “dark age”. As the universe is evolved, matter fluctuations grow gravitationally and dark matter is collapsed at over-dense region. Gravitational potential by collapsed objects attracts baryonic objects around dark matter halos and these baryonic objects form primordial stars (Yoshida et al. 2006). As a result of the formation of first stars, the period called “cosmic dawn” in which astrophysical processes play an important role begins (Fialkov et al. 2013; Visbal et al. 2012; Santos et al. 2011). After the first objects are formed, the spin temperature of neutral hydrogen couples to the color temperature of Lyman alpha ( $\text{Ly-}\alpha$ ) radiation emitted from the first objects. This effect is called “Wouthuysen Field (WF) effect” (Wouthuysen 1952). Typically,  $\text{Ly-}\alpha$  radiation field temperature is nearly equal to the kinetic temperature of intergalactic medium (IGM) because  $\text{Ly-}\alpha$  scattering rate is very large and the frequent scattering leads to a large number of  $\text{Ly-}\alpha$  photons which brings  $\text{Ly-}\alpha$  radiation field coupling to the gas which property is determined by

the kinetic temperature (Furlanetto et al 2006). Therefore, the spin temperature comes to couple to the kinetic temperature. After the WF effect becomes effective, next astrophysical process which affects the thermal history of IGM is X-ray heating (Pritchard & Furlanetto 2007). It is expected that cold IGM is heated due to the X-ray photons emitted from X-ray binaries (Fialkov et al 2014) and gas kinetic temperature increases dramatically (Mesinger et al 2012; Christian et al. 2013). As the heating of IGM progresses, thermal phase of IGM is changed and neutral hydrogen starts to be ionized by UV radiation from early galaxies (Loeb & Barkana 2001). This epoch is called “Epoch of Reionization (EoR)” (Fan et al. 2006).

The redshifted 21cm line from neutral hydrogen is sensitive to the thermal and ionized states of gas as well as the first objects in the early universe and it has been expected to give us valuable information about the thermal history of intergalactic medium (IGM) (Furlanetto et al 2006).

One of the statistical methods to probe the IGM state is the power spectrum of brightness temperature (21cm power spectrum) (Furlanetto et al 2006; Pritchard & Furlanetto 2007; Santos et al. 2008; Baek et al. 2010; Mesinger et al. 2013; Pober et al. 2014). Brightness temperature is a fundamental quantity of the 21cm signal, which is the spin temperature offsetting from the CMB temperature  $T_\gamma$  along the line of sight (LoS) at observed frequency  $\nu$ . This can be written as

(Furlanetto et al 2006)

$$\begin{aligned} \delta T_b(\nu) &= \frac{T_S - T_\gamma}{1+z} (1 - e^{-\tau_{\nu_0}}) \\ &\sim 27 x_H (1 + \delta_m) \left( \frac{H}{dv_r/dr + H} \right) \left( 1 - \frac{T_\gamma}{T_S} \right) \\ &\quad \times \left( \frac{1+z}{10} \frac{0.15}{\Omega_m h^2} \right)^{1/2} \left( \frac{\Omega_b h^2}{0.023} \right) [\text{mK}]. \end{aligned} \quad (1)$$

Here,  $T_S$  is gas spin temperature,  $\tau_{\nu_0}$  is the optical depth at the 21cm rest frame frequency  $\nu_0=1420.4\text{MHz}$ ,  $x_H$  is neutral fraction of the gas,  $\delta_m(\mathbf{x}, z) \equiv \rho/\bar{\rho} - 1$  is the evolved matter overdensity,  $H(z)$  is the Hubble parameter and  $dv_r/dr$  is the comoving gradient of the line of sight component of the comoving velocity of the gas. All quantities are evaluated at redshift  $z = \nu_0/\nu - 1$ .

On-going radio interferometers such as Murchison Wide Field Array (Tingay et al. 2012), Low Frequency Array (Rottgering et al. 2013) and Probing the Epoch of Reionization (Pober et al. 2014) have been operated as the “prototype” of future high-sensitivity experiments. Although the sensitivities of the on-going experiments are not enough to obtain the images of the redshifted 21cm line from the early universe, the power spectrum of the 21cm signal would be detected (Mesinger et al. 2013). In particular, it is expected that the 21cm power spectrum for each redshift ( $z = 10 \sim 30$ ) can be measured by Square Kilometre Array with high accuracy (Carilli 2014).

There have been numerous works about the 21cm power spectrum in both theoretical and observational aspects (Mao et al. 2008; Loeb et al 2008; Dillon et al 2013; Pober et al. 2014). In particular, most of such works have focused on the 21cm signal from the epoch of Reionization (EOR) at  $z \sim 6-10$ . In this epoch, the 21cm power spectrum is expected to trace the spatial distribution of the neutral fraction of gas  $x_H$  and we can ignore the fluctuation of the spin temperature because  $T_\gamma/T_S \ll 1$ . On the other hand, the 21cm signal from  $z \gtrsim 10-15$ , at when in the universe the first astrophysical objects have started to be formed, has not been investigated deeply (Ghara et al. 2014). This epoch is called as “cosmic dawn” and it should be also important to investigate the 21cm signal from the IGM at this epoch because the state of IGM at this epoch has to be crucial for the formation of the first astrophysical objects. At this epoch, since the reionization process has not proceeded sufficiently, the neutral fraction of gas  $x_H$  should be almost unity and the spatial distribution of the brightness temperature does not trace that of the neutral fraction. Instead of this, the 21cm power spectrum from this epoch should have the information about not only the matter density field but also the spin temperature related with the state of IGM.

In this work, we focus on the 21cm signal from the epoch of “cosmic dawn”, that is  $z \gtrsim 15$ , and investigate what we can learn from the signal by using a public code called 21cmFAST (Mesinger et al. 2007; Mesinger et al. 2011). This code is based on a semi-analytic model of star/galaxy formation and reionization. First, in order to find how physical processes are related to the observed 21cm signal at  $z \gtrsim 15$ , we decompose the 21cm power spectrum into three components composed by fluctuations of the matter density field, those of the neutral fraction and

those of the spin temperature, and discuss the redshift evolution of the power spectrum.

Next, we further focus on the distributions, variances and skewnesses of the brightness temperature and three decomposed components, in order to understand the physical meaning of the behavior of the 21cm power spectrum more deeply. Although there are several studies which discuss the one-point statistics of the brightness temperature (Harker et al. 2008; Watkinson & Pritchard 2013), most of such works have focused on the signal from EoR, that is,  $z \lesssim 10$ , to investigate its dependence on the reionization process, and for the signal from  $z \gtrsim 15$  the one-point statistics are not sufficiently discussed.

This paper is organized as follows. In section 2, first we show the 21cm power spectrum and the decomposition of it into each component and discuss the redshift dependence of the power spectrum. In section 3, we investigate distribution and one-point statistics such as variance and skewness of the spin temperature which is a dominant component of the 21cm power spectrum at higher redshift ( $z \gtrsim 15$ ), and also we investigate its dependence on the X-ray heating efficiency. In section 4, based on the discussion about the one-point statistics of the spin temperature given in section 3, we investigate the one-point statistics of observed brightness temperature. In section 5, we give a summary and conclusion.

Unless stated otherwise, we quote all quantities in comoving units. We employ the best fit values of the standard cosmological parameters obtained in (Komatsu et al. 2011).

## 2 EVOLUTION OF POWER SPECTRUM

In this section, we calculate the 21cm power spectrum and its decomposition into spectra of the matter density field, the neutral fraction and the spin temperature. In particular, we focus on the redshift evolution of the power spectra.

First, we define the power spectrum of brightness temperature as,

$$\langle \delta_{21}(\mathbf{k}) \delta_{21}(\mathbf{k}') \rangle = (2\pi)^3 \delta(\mathbf{k} + \mathbf{k}') P_{21}(\mathbf{k}), \quad (2)$$

where  $\delta_{21}(\mathbf{k}) \equiv \delta T_b(\mathbf{k}) / \langle \delta T_b \rangle - 1$  and  $\langle \delta T_b \rangle$  is the mean brightness temperature obtained from brightness temperature map. As we saw in Eq.(1), the fluctuation of brightness temperature is contributed from those in the matter density, spin temperature, neutral fraction and peculiar velocity. Here we define  $\delta_H$  and  $\delta_\eta$  such that  $x_H = \bar{x}_H(1 + \delta_H)$  and  $\eta = \bar{\eta}(1 + \delta_\eta)$  where  $\eta = 1 - T_\gamma/T_S$ ,  $\bar{x}_H, \bar{\eta}$  are volume average of  $x_H, \eta$  and the power spectra of  $\delta_m, \delta_H$  and  $\delta_\eta$  as,

$$\langle \delta_m(\mathbf{k}) \delta_m(\mathbf{k}') \rangle = (2\pi)^3 \delta(\mathbf{k} + \mathbf{k}') P_m(\mathbf{k}), \quad (3)$$

$$\langle \delta_H(\mathbf{k}) \delta_H(\mathbf{k}') \rangle = (2\pi)^3 \delta(\mathbf{k} + \mathbf{k}') P_{x_H}(\mathbf{k}), \quad (4)$$

$$\langle \delta_\eta(\mathbf{k}) \delta_\eta(\mathbf{k}') \rangle = (2\pi)^3 \delta(\mathbf{k} + \mathbf{k}') P_\eta(\mathbf{k}), \quad (5)$$

Here, we introduce a new parameter  $\eta$  in order to describe the fluctuation of the spin temperature  $T_S$ . By making use of this parameter, the brightness temperature can be related with the contribution of the spin temperature linearly. In the case where the fluctuation of the spin temperature  $\delta T_S (= (T_S - \bar{T}_S)/\bar{T}_S)$  is small,  $\delta_\eta$  and  $\delta_{T_S}$  are related as

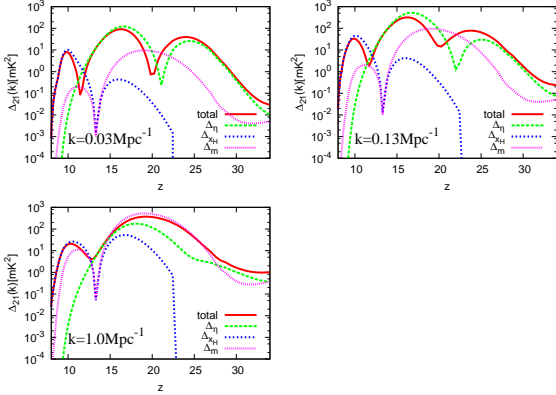


**Figure 1.** Total and decomposed 21cm power spectra as functions of the redshift for  $k = 0.03 \text{ Mpc}^{-1}$  (left top),  $0.13 \text{ Mpc}^{-1}$  (right top) and  $1.0 \text{ Mpc}^{-1}$  (left bottom).

$$\delta_\eta \simeq \frac{T_\gamma/\bar{T}_S}{1 - T_\gamma/\bar{T}_S} \delta T_S. \quad (6)$$

The cross correlations such as  $P_{x_H\eta}$  are defined in a similar way. Then, from Eq.(1), we see that the power spectrum of brightness temperature can be decomposed into a sum of the auto-correlations and cross-correlations:

$$P_{21} = (\bar{\delta T_b})^2 [P_m + P_{x_H} + P_\eta + P_{x_H\eta} + P_{x_Hm} + P_{m\eta}], \quad (7)$$

where,

$$\bar{\delta T_b} = 27\bar{x}_H \bar{\eta} [(1+z)/10]^{1/2} (0.15/\Omega_m h^2)^{1/2} (\Omega_b h^2/0.023).$$

We neglected higher-order terms and we have checked that the higher-order contributions are at most 30% of the total power spectrum at higher redshifts we are interested in here, and do not affect the qualitative feature of the redshift evolution. Therefore, the contribution can be safely neglected for the purpose of this article. However, for more precise quantitative discussion, such higher-order contributions have to be evaluated precisely. We plan to investigate the higher-order contribution and non-linearity in the future.

To compute the power spectra, we use a public code called 21cmFAST (Mesinger et al. 2007; Mesinger et al. 2011). This code is based on a semi-analytic model of star/galaxy formation and reionization, and outputs maps of matter density, velocity, spin temperature, ionized fraction and brightness temperature at the designated redshifts. We performed simulations in a  $(200\text{Mpc})^3$  comoving box with  $300^3$  grids, which corresponds to 0.66 Mpc resolution or  $\sim 3$  arcmin at 80 MHz ( $z=17$ ) (we show some telescope specifications in table.1), from  $z = 200$  to  $z = 8$  adopting the following parameter set,  $(\zeta, \zeta_X, T_{\text{vir}}, R_{\text{mfp}}) = (31.5, 10^{56}/M_\odot, 10^4 \text{ K}, 30 \text{ Mpc})$ . Here,  $\zeta$  is the ionizing efficiency,  $\zeta_X$  is the number of X-ray photons emitted by source per solar mass,  $T_{\text{vir}}$  is the minimum virial temperature of halos which produce ionizing photons, and  $R_{\text{mfp}}$  is the mean free path of ionizing photons through the IGM. In our calculation, we also ignore, for simplicity, the gradient of peculiar velocity whose contribution to the brightness temperature is relatively small (a few %) (Ghara et al. 2014).

In Fig. 1, we plot the total and decomposed power spectra,  $\Delta_i = k^3 P_i/2\pi^2$  with  $i = 21, x_H, m$  and  $\eta$ , as functions

of redshift for  $k = 0.03, 0.13, 1.0 \text{ Mpc}^{-1}$ . We can see several characteristic peaks in the total power spectrum: three peaks for  $k = 0.03, 0.13 \text{ Mpc}^{-1}$  and two peaks for  $k = 1.0 \text{ Mpc}^{-1}$ . These were already found in the previous works and it was suggested that they are, from high- $z$  one to low- $z$  one, induced by the WF effect, X-ray heating and reionization, respectively (Pritchard & Furlanetto 2007). Below we give a more detailed interpretation considering contributions from the fluctuations in neutral fraction, matter density and spin temperature.

First, the fluctuation in neutral fraction appears when reionization begins but power spectrum,  $(\bar{\delta T_b})^2 P_{x_H}$ , is subdominant at high redshifts ( $z \gtrsim 15$ ). It becomes dominant as reionization proceeds and forms the low- $z$  peak at  $z \approx 10$ . A dip at  $z \approx 14$  corresponds to the redshift when the average spin temperature becomes equal to the CMB temperature so that the average brightness temperature,  $\bar{\delta T_b}$ , vanishes. This dip is also seen in the contribution of matter fluctuations, which is important at smaller scales.

On the other hand, the power spectrum contributed from the spin-temperature fluctuations is negligible at low redshifts ( $z \lesssim 10$ ). This is because at these redshifts the spin temperature is much higher than the CMB temperature and the factor  $\eta = 1 - T_\gamma/\bar{T}_S$  is almost unity independent of the value of  $T_S$ . The spin-temperature fluctuations are important at higher redshifts ( $z \gtrsim 13$ ) especially at larger scales and this contribution forms the two peaks at  $z \approx 16$  and  $24$ . However, there are slight deviations in the peak positions between the brightness temperature and spin temperature due to the presence of matter fluctuations.

Thus, the low- $z$  peak and the other two peaks are contributed from the neutral fraction and spin temperature fluctuations, respectively, while the high- $z$  peak at small scales can not be seen due to the contribution from matter fluctuations. In other words, the evolution of spin temperature, which reflects the formation rate and properties of the first-generation stars, can be directly probed by measuring the power spectrum of brightness temperature at  $z \gtrsim 15$ . In the next section, we focus on the understanding of spin-temperature fluctuations at this epoch considering one-point statistics.

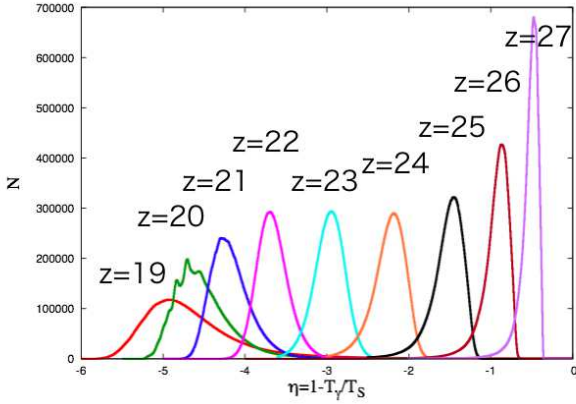
### 3 ONE-POINT STATISTICS OF SPIN TEMPERATURE

In this section, we study the probability distribution function (PDF) of spin temperature and one-point statistics such as variance and skewness. In practice, we focus on  $\eta = 1 - T_\gamma/\bar{T}_S$ , rather than  $T_S$  itself, because it is linearly related to the brightness temperature. However, because  $\eta$  is a monotonic function of  $T_S$ , physical interpretation is relatively straightforward. Recently, one-point statistics of brightness temperature during reionization was investigated assuming  $T_S \gg T_\gamma$  (Barkana & Loeb 2008; Harker et al. 2008; Watkinson & Pritchard 2013). This condition is not valid in our context.

Obtained maps of  $\eta$  from 21cmFAST for the redshifts  $z = 28, 25, 22$ , and  $19$  are shown in Fig. 3. From these maps, we evaluate the PDF and also the variance and skewness of

**Table 1.** Resolution at 80 MHz ( $z \sim 17$ ) (Dewdney et al 2013).

telescope	maximum baseline	spacial resolution	angle resolution
LOFAR	$\sim 1500$ m	$\sim 13$ Mpc	$\sim 4$ arcmin
MWA	$\sim 750$ m	$\sim 27$ Mpc	$\sim 9$ arcmin
SKA1	$\sim 2000$ m	$\sim 10$ Mpc	$\sim 3$ arcmin
SKA2	$\sim 5000$ m	$\sim 4$ Mpc	$\sim 1$ arcmin

**Figure 2.** PDF of  $1 - T_\gamma/T_S$  for  $z = 19 - 27$  obtained from the map of the spin temperature shown in Fig. 3.

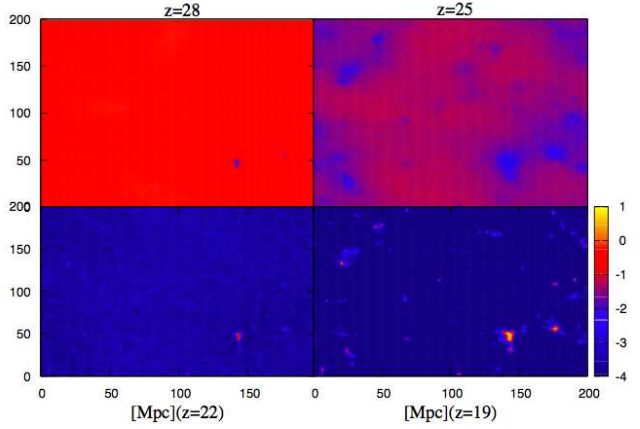
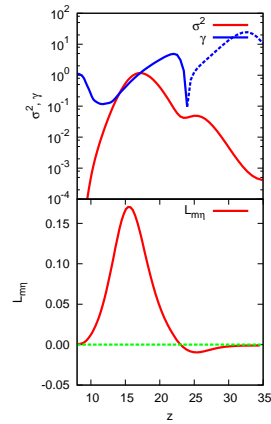
$\eta$ . The variance and skewness of a variable  $X$  are defined as,

$$\sigma^2 = \frac{1}{N} \sum_{i=1}^N [X - \bar{X}]^2 \quad (8)$$

$$\gamma = \frac{1}{N\sigma^3} \sum_{i=1}^N [X - \bar{X}]^3, \quad (9)$$

where  $N$  is the number of pixels of the maps. Note that the skewness is negative (positive) when the tail of the distribution relatively extends toward low (high) values of  $X$ .

We plot the PDF of  $\eta$  for  $z = 19 - 27$  in Fig. 2. First of all, the average value of  $\eta$  decreases as redshift decreases because the spin temperature strongly couples to the kinetic temperature, which decreases as  $(1+z)^2$  due to the adiabatic cooling of gas, via the WF effect at this epoch. Next, we see the shape of the PDF is also changing and, in particular, the direction of the longer tail changes at  $z \approx 23$  (cyan dot-dashed line). This is also confirmed in the top of Fig. 4, where we plot the time evolution of the variance and skewness of the PDF. Actually, the sign of the skewness changes at the same redshift from negative to positive. Here it is important to note that the variance has a local minimum at almost the same timing. Because the variance is the integration of the power spectrum with respect to the wavenumber, this local minimum corresponds to the dip in the contribution of  $\eta$  in Fig. 1.

**Figure 3.** The map of  $1 - T_\gamma/T_S$  at  $z = 28$  (left top), 25 (right top), 22 (left bottom), 19 (right bottom). We can see that the spatial averaged value of  $\eta$  decreases from  $z = 28$  to 19. A spatial distribution of  $\eta$  can be also seen in each panel.**Figure 4.** [top] Variance and skewness of  $1 - T_\gamma/T_S$  as functions of redshift. For the skewness (denoted as a blue line), the dashed part corresponds to the negative skewness ( $\gamma < 0$ ). [bottom] Cross correlation between  $\delta_m$  and  $\eta$  as a function of redshift. Green dashed line corresponds to  $L_{m\eta} = 0$ .



The above behavior can be understood by considering the X-ray heating of the gas. As we can see in Fig. 3, at higher redshifts ( $z \gtrsim 25$ ) the spin temperature in the neighborhood of stars approaches to the kinetic temperature due to the WF effect and becomes lower than the average, and consequently its PDF has a tail toward lower temperature. Then, as X-ray heating becomes effective, the spin temperature increases in the neighborhood of stars and the tail goes toward higher-value side. At the transition time, the tail becomes shortest and consequently the variance has a local minimum there.

The bottom of Fig. 4, the cross correlation between the matter and spin temperature fluctuations, strongly supports the above interpretation. Here we evaluate the cross correlation from the cross power spectrum as

$$L_{m\eta} := \int \frac{d^3k}{(2\pi)^3} P_{m\eta}(k). \quad (10)$$

At higher redshifts ( $z \gtrsim 23$ ), the correlation is negative, that is, high-density regions have lower spin temperature. This would be due to the WF effect. On the other hand, at lower redshifts ( $z \lesssim 23$ ), as is expected from the interpretation that X-ray heating is effective here, the correlation is positive. It is seen that the cross correlation changes the sign at the same redshift as the skewness.

Finally, we vary the number of X-ray photons emitted per solar mass,  $\zeta_X$  (Mesinger et al 2012), and see the one-point statistics again. We take  $\zeta_X = 10^{55} M_\odot^{-1}, 10^{56} M_\odot^{-1}$  (fiducial value), and  $10^{57} M_\odot^{-1}$ , fixing the other parameters. The left top of Fig. 5 is the thermal history and we see that the spin temperature rises earlier for larger  $\zeta_X$ . The other panels of Fig. 5 show the evolution of the variance and skewness of the PDF of  $\eta$ , and the cross correlation between matter and  $\eta$  fluctuations. As  $\zeta_X$  increases, the critical redshift where the variance has a local minimum and the sign of the skewness and cross correlation changes increases. This is the expected behavior from our interpretation given in the previous section because X-ray heating will become effective earlier for larger  $\zeta_X$ . The power spectra of the brightness temperature contributed from the fluctuations in  $\eta$  are plotted in Fig. 6 and, as expected again, the dip appears earlier for larger  $\zeta_X$ .

In summary, the dip in the evolution of power spectrum contributed from the spin temperature fluctuations can be understood as the state that X-ray heating is effective. The transition occurs at  $z \approx 23$  for a fiducial set of model parameters and this depends on the effectiveness of X-ray heating. Conversely, our interpretation implies that, if we detect a dip in the redshift dependence of the power spectrum at the relatively higher redshift, we could know the redshift when X-ray begins to become effective. Further, when we detect a peak, it would be possible to know whether X-ray heating is effective at the redshift from the skewness. However, although the spin-temperature fluctuations are dominant at large scales, the contribution from matter fluctuations is not negligible and change the critical redshift as we see in the next section.

Here, it is important to note the difference between the redshift of the local minimum of the average spin temperature and the above critical redshift. The difference is due to the fact that the average spin temperature is a global property of the intergalactic gas while the skewness

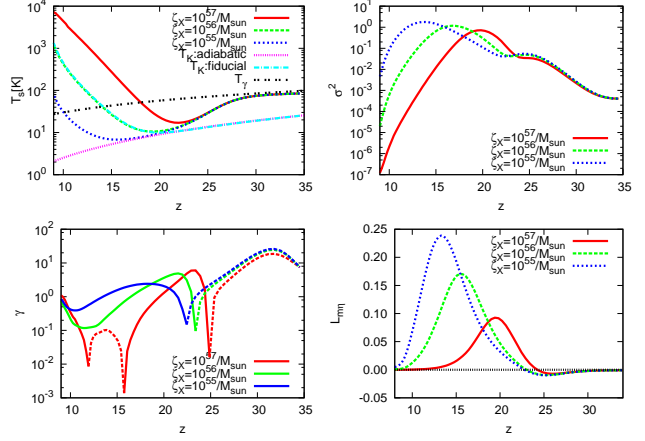


**Figure 5.** [left top] Spin temperature evolution for  $\zeta_X = 10^{57} M_\odot^{-1}$  (red),  $10^{56} M_\odot^{-1}$  (green) and  $10^{55} M_\odot^{-1}$  (blue). We also plot kinetic temperature in the absence of X-ray heating (pink) and in the presence of X-ray heating with  $\zeta_X = 10^{56} M_\odot^{-1}$  (light blue) and CMB temperature (black). [right top and left bottom] Evolution of variance and skewness of the probability distribution function of  $1 - T_\gamma/T_S$  for  $\zeta_X = 10^{57} M_\odot^{-1}$  (red),  $10^{56} M_\odot^{-1}$  (green) and  $10^{55} M_\odot^{-1}$  (blue). [right bottom] Cross correlation between  $\delta_m$  and  $\delta_\eta$  for  $\zeta_X = 10^{57} M_\odot^{-1}$  (red),  $10^{56} M_\odot^{-1}$  (green) and  $10^{55} M_\odot^{-1}$  (blue).

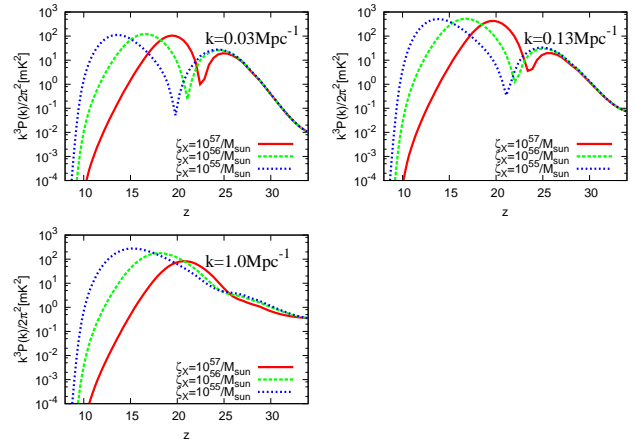


**Figure 6.** Power spectra of the brightness temperature contributed from the fluctuations in  $1 - T_\gamma/T_S$  for  $\zeta_X = 10^{57} M_\odot^{-1}$  (red),  $10^{56} M_\odot^{-1}$  (green) and  $10^{55} M_\odot^{-1}$  (blue) at three wave numbers as functions of redshift.

is largely affected by the behavior of a small fraction of gas near stars. Thus, the latter is more sensitive to the onset of X-ray heating. If so, it is expected that the difference in the two redshifts depends on the spectrum of X-ray (Fialkov et al 2014). For example, if the X-ray spectrum is hard, the difference will become smaller because higher-energy X-rays have larger mean free path so that they tend to heat larger region around the source.

#### 4 ONE-POINT STATISTICS OF BRIGHTNESS TEMPERATURE

In this section, we focus on the one point statistics of the brightness temperature. The variance and skewness of brightness temperature are described by

$$\sigma_{\delta T_b} = \langle \overline{\delta T_b} \rangle^2 [\sigma_{\delta_m} + \sigma_{\delta_\eta} + \sigma_{\delta_{x_H}} + \langle \delta_m \delta_\eta \rangle + \langle \delta_m \delta_{x_H} \rangle + \langle \delta_\eta \delta_{x_H} \rangle + O(\delta^3)]. \quad (11)$$

$$\gamma_{\delta T_b} = \langle \overline{\delta T_b} \rangle^3 [\gamma_{\delta_m} + \gamma_{\delta_\eta} + \gamma_{\delta_{x_H}} + \langle \delta_m \delta_\eta \delta_{x_H} \rangle + 3(\langle \delta_m^2 \delta_\eta \rangle + \langle \delta_m^2 \delta_{x_H} \rangle + \langle \delta_\eta^2 \delta_{x_H} \rangle + \langle \delta_m \delta_\eta^2 \rangle + \langle \delta_m \delta_{x_H}^2 \rangle + \langle \delta_\eta \delta_{x_H}^2 \rangle) + O(\delta^4)]. \quad (12)$$

Here, we notice that  $\overline{\delta T_b}$  is slightly different from the average  $\langle \delta T \rangle$  obtained from brightness temperature map due to the contribution of higher-order terms. Although we focus on relatively high redshift, we find that  $\delta_{x_H}$  is important when we consider the skewness.

In Fig.7, we plot the variance and skewness of brightness temperature with their components. Comparing the variance with skewness, we find that neutral-fraction fluctuation  $\delta_{x_H}$  is not negligible in skewness at  $z \leq 20$ , although it does not contribute to the total variance so much. As you can see in the bottom of Fig. 7, the change of sign in skewness for the brightness temperature is deviated from the one of  $\eta$  due to the contribution of matter fluctuations, which have always negative skewness. Nonetheless, the skewness is still a good indicator to study the epoch when X-ray heating becomes effective. We note here that the non-linear terms in skewness is the same order as the linear terms but qualitative behavior does not change whether we include non-linear terms or not.

#### 5 SUMMARY & DISCUSSION

In this paper, we gave a physical interpretation of the evolution of the power spectrum of the 21cm brightness temperature during the Cosmic Dawn and the Epoch of Reionization using a public code, 21cmFAST. With a fixed wave number, the power spectrum has three peaks as a function of redshift. First, we decomposed the power spectrum into those contributed from the fluctuations in dark matter density, spin temperature and neutral fraction and found that the peak with the lowest redshift is mostly contributed from the neutral fraction, while the other two peaks are contributed from the dark matter density and spin temperature fluctuations. Further, it was found that a dip between two peaks with higher redshifts is induced by the neutral fraction. Then, to understand the physical meaning of the dip, we investigated the one-point function of the spin temperature distribution. We found that the redshift of the dip is critical in a sense that the skewness of the one-point function and the correlation coefficient between the spin temperature and dark matter distribution change their signs and that the variance also has a dip. From this fact, it was implied that the dip in the power spectrum of the brightness temperature contributed from the spin temperature is a signature of the onset of X-ray heating of the gas. This interpretation was justified

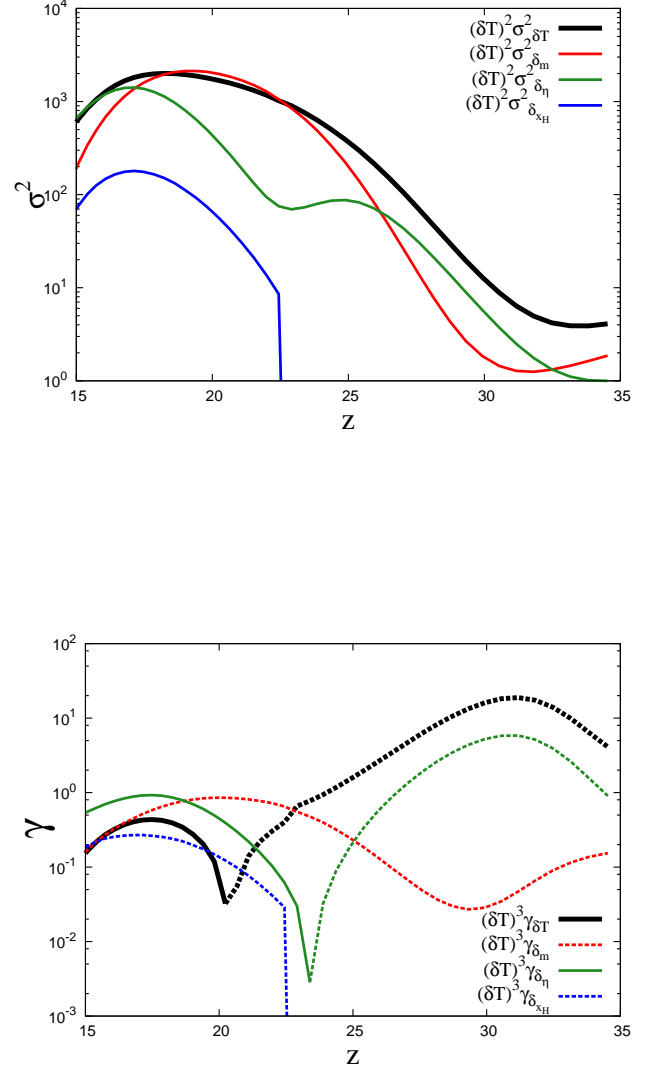


**Figure 7.** [Top] The variance of brightness temperature (black), of  $\delta_m$  (red), of  $\delta_\eta$  (green), of  $\delta_{x_H}$  (blue). [Bottom] the skewness of brightness temperature (black), of  $\delta_m$  (red), of  $\delta_\eta$  (green), of  $\delta_{x_H}$  (blue). Dashed part corresponds to negative value and solid part corresponds to positive value. All quantities are multiplied  $(\overline{\delta T_b})^2$  (variance) or  $(\overline{\delta T_b})^3$  (skewness).

by seeing the behavior when varying the model parameter corresponding to X-ray heating.

Due to the contribution of dark matter density, the redshift of the dip in the power spectrum contributed from the spin temperature is slightly different from that in the full power spectrum. However, the dip will still be a good indicator of the onset of X-ray heating. Further, based on the cosmological perturbation theory, we can theoretically estimate the skewness of the brightness temperature contributed from the dark matter fluctuations in the standard

cosmological model. Therefore, in principle, we can subtract the dark matter contribution and directly measure the skewness of the contribution from the spin temperature. Moreover, the scale dependence of the bispectrum, which has a close relation to the skewness, of the brightness temperature would help us to extract the information about the spin temperature from the observed brightness temperature. The bispectrum is also deeply related to the non-linear terms (Litz et al. 2007) in the power spectrum which we neglected in this paper. Because the fluctuations in the spin temperature are of order  $\sim O(0.1)$  and are deviated from Gaussian distribution, the non-linear terms are potentially important. In particular, we found that the linear and non-linear terms are comparable when we evaluate the skewness. Further, the bispectrum and higher-order statistics would be very useful to extract physical information from 21cm signal (Pillepich et al. 2006; Cooray 2005; Cooray et al. 2008), as mentioned above. These topics will be presented elsewhere.

The detectability of variance and skewness was discussed in (Harker et al. 2008; Jelić et al. 2008; Watkinson & Pritchard 2013). Following (Watkinson & Pritchard 2013), the signal-to-noise ratio,  $S/N$ , of skewness can be roughly estimated by

$$S/N \sim \sqrt{\frac{\gamma^2 \sigma^3}{\sigma_{\text{noise}}^6 / N_{\text{pix}}}}, \quad (13)$$

where we have neglected the contribution from kurtosis. Here,  $N_{\text{pix}}$  is the number of pixels and we set  $N_{\text{pix}} = 300^3$  and  $\sigma_{\text{noise}}$  is the instrumental noise on brightness temperature given by

$$\begin{aligned} \sigma_{\text{noise}} &= 0.37 \text{mK} \left( \frac{10^6 \text{m}}{A_{\text{tot}}} \right) \left( \frac{5'}{\Delta\theta} \right)^2 \left( \frac{1+z}{10} \right)^{4.6} \\ &\times \sqrt{\left( \frac{1 \text{MHz}}{\Delta\nu} \frac{1000 \text{hours}}{t_{\text{int}}} \right)}, \end{aligned} \quad (14)$$

where  $A_{\text{tot}}$  is the total effective area of array,  $\theta$  is angular resolution,  $\Delta\nu$  is frequency resolution and  $t_{\text{int}}$  is observing time. Considering the SKA1 ( $A_{\text{tot}} = 4 \times 10^5 [\text{m}^2]$ ) and SKA2 ( $A_{\text{tot}} = 3 \times 10^6 [\text{m}^2]$ ) with 1000 hours of observation time and  $\Delta\nu \sim 0.1 \text{MHz}$ , we obtain  $S/N = 6$  and  $18$  at  $z = 15$ , and  $S/N = 2$  and  $8$  at  $z = 20$ , for SKA1 and SKA2, respectively.

Finally, we would like to note that the variance and skewness are actually dependent on the angular resolution and survey area. This can be understood by the fact that they are expressed by the integration of power spectrum and bispectrum with respect to the wavenumber. In our calculation, we have fixed the box size and the number of grids in simulations to be  $(200 \text{ Mpc})^3$  and  $300^3$ , respectively. This is corresponding to  $0.66 \text{ Mpc}$  resolution or  $\sim 3 \text{ arcmin}$  at  $80 \text{ MHz}$  ( $z = 17$ ). In Fig. 8, we show the evolution of skewness of brightness temperature with varying the spacial resolution  $0.66, 1.3$  and  $2.0 \text{ Mpc}$ . These correspond to  $3 \text{ arcmin}$ ,  $6 \text{ arcmin}$ ,  $9 \text{ arcmin}$ . and fixing the box size. The lowest resolution roughly corresponds to that of the SKA2. It is seen that the peak at  $z \sim 18$  is diminished for higher resolution, while the one at  $z \sim 30$  is not affected. On the other hand, the change of sign is shifted slightly to higher redshift for higher resolution. More detailed study on the dependence of skewness on the resolution needs the understanding of the

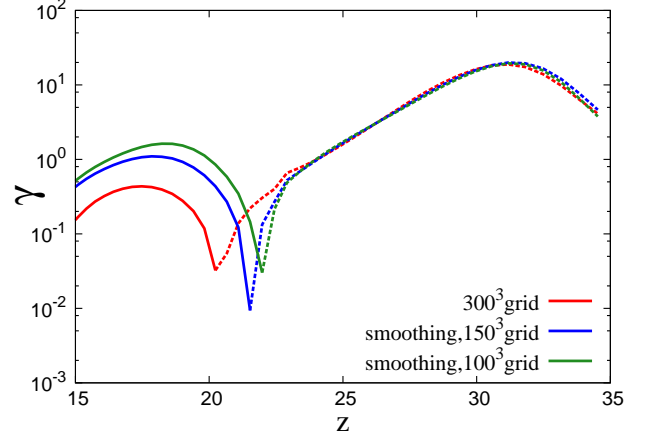


**Figure 8.** Skewness evolution of the brightness temperature varying the number of grids:  $300^3$  (fiducial, red),  $150^3$  (blue) and  $100^3$  (green). The latter two cases are calculated by smoothing the fiducial model.

bispectrum of the brightness temperature fluctuations and this will be presented elsewhere.

## ACKNOWLEDGEMENT

We would like to thank K. Hasegawa for useful comments. This work is supported by Grant-in-Aid from the Ministry of Education, Culture, Sports, Science and Technology (MEXT) of Japan, Nos. 24340048 (K.T. and K.I.) and 26610048. (K.T.), No. 25-3015 (H.S.) and No. 24-2775 (S.Y.).

## REFERENCES

- P. A. R. Ade *et al.* [Planck Collaboration], arXiv:1303.5084 [astro-ph.CO].
- S. Baek, B. Semelin, P. Di Matteo, Y. Revaz and F. Combes, arXiv:1003.0834 [astro-ph.CO].
- R. Barkana, & A. Loeb, 2008, MNRAS, 384, 1069
- N. Bartolo, E. Komatsu, S. Matarrese and A. Riotto, Phys. Rept. **402**, 103 (2004) [astro-ph/0406398].
- C. L. Carilli, arXiv:1408.5317 [astro-ph.IM].
- P. Christian and A. Loeb, JCAP **1309** (2013) 014 [arXiv:1305.5541 [astro-ph.CO]].
- A. Cooray, Mon. Not. Roy. Astron. Soc. **363** (2005) 1049 [astro-ph/0411430].
- A. Cooray, C. Li and A. Melchiorri, Phys. Rev. D **77** (2008) 103506 [arXiv:0801.3463 [astro-ph]].
- P. Dewdney *et al* <http://www.skatelescope.org/wp-content/uploads/2013/04/SKA-Phase-2-Design-Report-2013-04-22.pdf>
- J. S. Dillon, A. Liu, C. L. Williams, J. N. Hewitt, M. Tegmark, E. H. Morgan, A. M. Levine and M. F. Morales *et al.*, Phys. Rev. D **89**, 023002 (2014) [arXiv:1304.4229 [astro-ph.CO]].

- X. H. Fan, C. L. Carilli and B. G. Keating, *Ann. Rev. Astron. Astrophys.* **44** (2006) 415 [astro-ph/0602375].
- A. Fialkov, R. Barkana, A. Pinhas and E. Visbal, arXiv:1306.2354 [astro-ph.CO].
- A. Fialkov, R. Barkana and E. Visbal, arXiv:1402.0940 [astro-ph.CO].
- S. Furlanetto, S. P. Oh and F. Briggs, *Phys. Rept.* **433** (2006) 181 [astro-ph/0608032].
- R. Ghara, T. R. Choudhury and K. K. Datta, arXiv:1406.4157 [astro-ph.CO].
- G. J. A. Harker, S. Zaroubi, R. M. Thomas, V. Jelic, P. Labropoulos, G. Mellema, I. T. Iliev and G. Bernardi *et al.*, arXiv:0809.2428 [astro-ph].
- Jelić, V., Zaroubi, S., Labropoulos, P., et al. 2008, *MNRAS*, **389**, 1319
- E. Komatsu *et al.* [WMAP Collaboration], *Astrophys. J. Suppl.* **192** (2011) 18 [arXiv:1001.4538 [astro-ph.CO]].
- A. Lidz, O. Zahn, M. McQuinn, M. Zaldarriaga and S. Dutta, *Astrophys. J.* **659** (2007) 865 [astro-ph/0610054].
- A. Loeb and R. Barkana, *Ann. Rev. Astron. Astrophys.* **39**, 19 (2001) [astro-ph/0010467].
- A. Loeb and S. Wyithe, *Phys. Rev. Lett.* **100**, 161301 (2008) [arXiv:0801.1677 [astro-ph]].
- Y. Mao, M. Tegmark, M. McQuinn, M. Zaldarriaga and O. Zahn, *Phys. Rev. D* **78**, 023529 (2008) [arXiv:0802.1710 [astro-ph]].
- G. Mellema, L. V. E. Koopmans, F. A. Abdalla. et al 2013, *Experimental Astronomy*, **36**, 235
- A. Mesinger and S. Furlanetto, arXiv:0704.0946 [astro-ph].
- A. Mesinger, S. Furlanetto, R. Cen, 2011, *MNRAS*, **411**, 955
- A. Mesinger, A. Ferrara and D. S. Spiegel, arXiv:1210.7319 [astro-ph.CO].
- A. Mesinger, A. Ewall-Wice and J. Hewitt, arXiv:1310.0465 [astro-ph.CO].
- A. Pillepich, C. Porciani and S. Matarrese, *Astrophys. J.* **662** (2007) 1 [astro-ph/0611126].
- D. C. J. J. C. Pober, A. R. Parsons, J. E. Aguirre, Z. Ali, J. Bowman, R. F. Bradley, C. L. Carilli and D. R. DeBoer *et al.*, arXiv:1408.3389 [astro-ph.CO].
- J. C. Pobe, A. Liu, A. J. S. Dillon, et al. 2014, *ApJ*, **782**, 66
- J. R. Pritchard and S. R. Furlanetto, *Mon. Not. Roy. Astron. Soc.* **376** (2007) 1680 [astro-ph/0607234].
- H. Rottgering, *New Astron. Rev.* **47** (2003) 405 [astro-ph/0309537].
- M. G. Santos, A. Amblard, J. Pritchard et al. 2008, *ApJ*, **689**, 1
- M. G. Santos, M. B. Silva, J. R. Pritchard, R. Cen, & A. Cooray. 2011, *A & A*, **527**, A93
- S. J. Tingay, R. Goeke, J. D. Bowman, D. Emrich, S. M. Ord, D. A. Mitchell, M. F. Morales and T. Booler *et al.*, arXiv:1206.6945 [astro-ph.IM].
- E. Visbal, R. Barkana, A. Fialkov, D. Tselikhovich and C. Hirata, arXiv:1201.1005 [astro-ph.CO].
- C. A. Watkinson and J. R. Pritchard, *Mon. Not. Roy. Astron. Soc.* **443**, 3090 (2014) [arXiv:1312.1342 [astro-ph.CO]].
- S. A. Wouthuysen, *Astronomical Journal*, **57**, 31
- N. Yoshida, K. Omukai, L. Hernquist, & T. Abel 2006, *ApJ*, **652**, 6